
High dimensional theory of two-phase optimizers

Atish Agarwala¹

Abstract

The trend towards larger training setups has brought a renewed interest in partially asynchronous two-phase optimizers which optimize locally and then synchronize across workers. Additionally, recent work suggests that the one-worker version of one of these algorithms, DiLoCo, shows promising results as a (synchronous) optimizer. Motivated by these studies we present an analysis of LA-DiLoCo, a simple member of the DiLoCo family, on a high-dimensional linear regression problem. We show that the one-worker variant, LA, provides a different trade-off between signal and noise than SGD, which is beneficial in many scenarios. We also show that the multi-worker version generates more noise than the single worker version, but that this additional noise generation can be ameliorated by appropriate choice of hyperparameters. We conclude with an analysis of SLA–LA with momentum – and show that stacking two momentum operators gives an opportunity for acceleration via a non-linear transformation of the “effective” Hessian spectrum, which is maximized for Nesterov momentum. Altogether our results show that two-phase optimizers represent a fruitful new paradigm for understanding and improving training algorithms.

1. Introduction

The success of deep learning has brought a pressing need for training algorithms that operate at scale, due to the desire to train larger models with larger and more complex datasets for longer time. Most progress in this area has been made by synchronous systems, which compute gradients across multiple machines but sync them before changing parameters. However, the cost of operating synchronous systems can grow superlinearly with scale due to issues like memory, communications bandwidth, and hardware failures.

¹Google DeepMind. Correspondence to: Atish Agarwala <thetish@google.com>.

Preprint. March 31, 2026.

This has led to numerous attempts to develop asynchronous training systems. While fully asynchronous training remains challenging, an intermediate approach is to design distributed optimizers where groups of workers maintain in-group synchrony, but between group synchronization takes a longer time (McMahan et al., 2017; Charles & Konečný, 2021). This allows for more flexible hardware configurations, and the possibility for more compute to be brought to bear on a single training run.

Recent work suggests that a two-phase optimization framework is a promising approach (Reddi et al., 2021; Malinovsky et al., 2020; Charles & Konečný, 2021; Charles & Rush, 2022; Khaled et al., 2025). Workers first perform an *inner optimization* using algorithms (e.g. SGD), and generate a *pseudo-gradient* — the difference between the parameters at the start and end of the inner optimization. These pseudo-gradients are then averaged and sent to an *outer optimizer* (e.g. SGD momentum) and used to perform a single optimization step — the results of which are sent to the workers as the starting point for the new inner optimization.

Douillard et al. (2023) show that one particular configuration of this two-phase framework, DiLoCo, exhibits promising results in distributed LLM training, a fact which has since been repeatedly observed empirically (Jaghour et al., 2024; Douillard et al., 2025; Charles et al., 2025), but the theoretical underpinnings of this performance remain mysterious. Even more surprising is the fact that DiLoCo shows benefits in the one-worker (synchronous) setting (Charles et al., 2025). There is even less theoretical understanding of this phenomenon, with some conjectures that the benefits are due to implicit regularization of the algorithms (Kallusky et al., 2025).

In this work we provide theoretical evidence that two-phase algorithms like DiLoCo provide *direct benefits to optimization itself*. We use tools from high-dimensional learning dynamics theory to exactly analyze the most basic algorithm in this class, Lookahead (LA) (Zhang et al., 2019), as well as the multi-worker version LA-DiLoCo (with outer optimizer SGD), and write an evolution equation for the expected value of the loss, which concentrates in high dimensions. We show the following:

- The combination of two optimizers induces a noise structure that is quantitatively different from SGD.
- LA allows a different tradeoff between signal and noise than SGD, and in some scenarios is provably better than SGD at optimal learning rates.
- LA-DiLoCo generates more noise in the distributed setting than the synchronous setting, but there are hyperparameter choices which minimize the discrepancy between the methods for small number of workers.

We then provide analysis of the extension Super Lookahead (SLA) — LA with momentum in the inner and outer optimizer. In the deterministic setting, we prove some key features of stacking momentum operators:

- The outer momentum operates on an “effective spectrum” generated by the inner optimizer, non-linearly transforming the relationship between Hessian eigenvalues and convergence rate.
- Nesterov-style momentum has large benefits over heavy ball momentum in this setting.

Our analysis suggests that there is a rich family of behaviors induced by LA and SLA which can’t be captured by more traditional algorithms and is worth further experimental and theoretical study.

2. Basics of high-dimensional linear regression

We introduce the high-dimensional linear regression setup studied previously (Lee et al., 2022; Agarwala & Pennington, 2024). We will present known results for the dynamics of SGD in this setting, so we can build on them to analyze the LA optimizer.

Consider a scenario with D targets \mathbf{y}_{tr} that we are trying to fit with a linear model with a P dimensional parameter vector $\boldsymbol{\theta}$ given by

$$f(\boldsymbol{\theta}) = \mathbf{y}_0 + \mathbf{J}\boldsymbol{\theta} \quad (1)$$

Here \mathbf{J} is the $D \times P$ dimensional Jacobian. We consider minimization of the MSE objective

$$\mathcal{L}(\boldsymbol{\theta}) = \frac{1}{2D} \|\mathbf{z}\|^2, \quad \mathbf{z} \equiv \mathbf{f}(\boldsymbol{\theta}) - \mathbf{y}_{tr}. \quad (2)$$

where we have defined the residuals \mathbf{z} for convenience. Previous works studied mini-batch SGD, where B examples are sampled from the D total datapoints in order to compute the gradient. The update rule for SGD in this setting is given by

$$\boldsymbol{\theta}_{t+1} - \boldsymbol{\theta}_t = -\frac{\eta}{B} \mathbf{J}^\top \mathbf{P}_t \mathbf{z}_t. \quad (3)$$

where \mathbf{P}_t is a $D \times D$ projection matrix, diagonal with B entries with value 1, and the rest 0, chosen at random. The \mathbf{P}_t are i.i.d. for different t . One feature of this model is that the updates close in function space. The residuals evolve as

$$\mathbf{z}_{t+1} - \mathbf{z}_t = -\eta \frac{D}{B} \hat{\Theta} \mathbf{P}_t \mathbf{z}_t. \quad (4)$$

where we define the empirical NTK $\hat{\Theta} \equiv \frac{1}{D} \mathbf{J} \mathbf{J}^\top$.

This means that it is possible to write the exact evolution of the moments of \mathbf{z} . For example, the first moment is given by

$$\begin{aligned} \mathbb{E}_{\mathbf{P}}[\mathbf{z}_{t+1} - \mathbf{z}_t | \mathbf{z}_t, \mathbf{J}_t] &= -\eta \hat{\Theta} \mathbf{z}_t \\ \mathbb{E}_{\mathbf{P}}[\mathbf{z}_{t+s}] &= \left(\mathbf{I} - \eta \hat{\Theta}\right)^s \mathbf{z}_t, \end{aligned} \quad (5)$$

which is equivalent to the evolution at full batch size.

The dynamics of the second moment can also be computed exactly (see Equation 7 and Appendix A.2 of Agarwala & Pennington (2024)). Since we are training on MSE loss, computing the diagonal of the covariance $\mathbb{E}_{\mathbf{P}}[\mathbf{z}_{t+1} \mathbf{z}_{t+1}^\top]$ would give us the expected loss trajectory. In the high dimensional limit ($B \gg 1$, $D \gg 1$, $B/D = O(1)$), Lee et al. (2022) showed that under appropriate conditions on $\hat{\Theta}$, the dynamics of the second moment simplify considerably and the loss trajectories concentrate. We recap the concentration results in the notation of Agarwala & Pennington (2024), to ease later exposition. Given the eigen-decomposition $\hat{\Theta} = \mathbf{V} \boldsymbol{\Lambda} \mathbf{V}^\top$, where \mathbf{V} is orthogonal and $\boldsymbol{\Lambda}$ is diagonal and PSD, we define the normalized diagonal $\mathbf{p}_t \equiv \boldsymbol{\Lambda}^\dagger \text{diag}(\mathbf{V}^\top \mathbb{E}_{\mathbf{P}}[\mathbf{z}_t \mathbf{z}_t^\top] \mathbf{V})$. In the limit, \mathbf{p} evolves as

$$\begin{aligned} \mathbf{p}_{t+1} &= (\mathbf{A} + \mathbf{B}) \mathbf{p}_t, \quad \mathbf{A} \equiv (\mathbf{I} - \eta \boldsymbol{\Lambda})^2, \\ \mathbf{B} &\equiv \left(\frac{1}{B} - \frac{1}{D}\right) \eta^2 \boldsymbol{\Lambda} \mathbf{1} \mathbf{1}^\top \boldsymbol{\Lambda}. \end{aligned} \quad (6)$$

The \mathbf{A} term corresponds to the deterministic dynamics of full batch training, and the \mathbf{B} term controls the noise, which is larger for small batch size B .

This system of equations can be used to derive quantities like the stochastic edge of stability — the critical learning rate above which dynamics diverges due to noise accumulation. Note that the loss is given simply by $\mathcal{L}(\boldsymbol{\theta}) = \frac{1}{D} \mathbf{1}^\top \boldsymbol{\Lambda} \mathbf{p}$.

3. Stochastic dynamics of LA-DiLoCo

We use the model and analysis technique described in the previous section and extend them to understand LA-DiLoCo. We first study LA, the one-worker case of LA-DiLoCo, and prove that in this setting the two-tier dynamics of LA can reduce the loss faster than SGD with optimal learning rate. We then study the multi-worker case, and analyze how the number of workers reshapes the dynamics of the noise.

3.1. Lookahead in the high-dimensional regime

We first analyze the lookahead (LA) algorithm, first introduced in Zhang et al. (2019). This is one of the most basic training algorithms compatible with the DiLoCo framework, but has only one worker. Given a sync time S , the update rule is given by:

$$\psi_t := \theta_t \text{ (when } t//S = 0) \quad (7)$$

$$\psi_{t+1} - \psi_t = -\eta \mathbf{g}_t(\psi_t) \text{ for } S \text{ steps} \quad (8)$$

$$\theta_{t+S} - \theta_t = \nu(\psi_{t+S} - \theta_t) \quad (9)$$

where \mathbf{g}_t is the minibatch gradient. In other words, there is an inner optimizer that applies SGD to a copy ψ of θ_t for S steps with *inner learning rate* η , after which an outer optimizer applies SGD based on the difference $\psi_{t+S-1} - \theta_t$ with *outer learning rate* ν . For $\nu = 1$ this corresponds to regular SGD, and for $\nu = 0$ this corresponds to no change to the parameters at all.

In the high dimensional linear model, the gradient is $\mathbf{J}^\top \mathbf{P}_t \mathbf{z}_t(\psi_t)/B$ and the algorithm can again be written entirely in function space:

$$\tilde{\mathbf{z}}_t := \mathbf{z}_t \text{ (when } t//S = 0) \quad (10)$$

$$\tilde{\mathbf{z}}_{t+1} - \tilde{\mathbf{z}}_t = -\eta \frac{D}{B} \hat{\Theta} \mathbf{P}_t \tilde{\mathbf{z}}_t \text{ for } S \text{ steps} \quad (11)$$

$$\mathbf{z}_{t+S} - \mathbf{z}_t = \nu(\tilde{\mathbf{z}}_{t+S} - \mathbf{z}_t) \quad (12)$$

with the definitions

$$\mathbf{z}_t \equiv f(\theta_t) - \mathbf{y}_{tr}, \tilde{\mathbf{z}}_t \equiv f(\psi_t) - \mathbf{y}_{tr} \quad (13)$$

This function space picture allows a direct extension of Equation 6 to LA. Computing the second moments of \mathbf{z}_t after a single cycle of S steps, we have:

$$\begin{aligned} \mathbb{E}[\mathbf{z}_{t+S} \mathbf{z}_{t+S}^\top | \mathbf{z}_t \mathbf{z}_t^\top] &= \mathbb{E}[\nu \tilde{\mathbf{z}}_{t+S} + (1-\nu) \mathbf{z}_t \\ &\quad [\nu \tilde{\mathbf{z}}_{t+S} + (1-\nu) \mathbf{z}_t]^\top | \mathbf{z}_t] \end{aligned} \quad (14)$$

Here the expectation is taken over the sequence of sampling matrices $\{\mathbf{P}_t, \mathbf{P}_{t+1}, \dots, \mathbf{P}_{t+S-1}\}$.

The $\tilde{\mathbf{z}}_{t+S}$ are the result of S steps of SGD, which means the terms can be computed in terms of the moments for SGD:

$$\mathbb{E}[\tilde{\mathbf{z}}_{t+S} \mathbf{z}_t^\top | \mathbf{z}_t \mathbf{z}_t^\top] = \boldsymbol{\mu}_{t,S} \mathbf{z}_t^\top, \boldsymbol{\mu}_{t,S} \equiv \mathbb{E}_{\text{SGD}}[\mathbf{z}_{t+S} | \mathbf{z}_t] \quad (15)$$

$$\mathbb{E}_{\mathbf{P}}[\tilde{\mathbf{z}}_{t+S} \tilde{\mathbf{z}}_{t+S}^\top | \mathbf{z}_t] = \mathbb{E}_{\text{SGD}}[\mathbf{z}_{t+S} \mathbf{z}_{t+S}^\top | \mathbf{z}_t] \quad (16)$$

Using these equations, we can compute the dynamics of the second moment eigenmodes in the high-dimensional limit of Lee et al. (2022) (Appendix A.1):

$$\begin{aligned} \mathbf{p}_{t+S} &= ([(1-\nu) \mathbf{I} + \nu (\mathbf{I} - \eta \mathbf{A})^S]^2 + \\ &\quad \nu^2 [\mathbf{T}_S - (\mathbf{I} - \eta \mathbf{A})^{2S}]) \mathbf{p}_t, \mathbf{T}_k \equiv (\mathbf{A} + \mathbf{B})^k \end{aligned} \quad (17)$$

The first term corresponds to the deterministic dynamics of LA. The second term can then be interpreted as the dynamical contribution of noise after S steps of SGD, and generally slows convergence rate relative to the deterministic setting.

We immediately see that LA allows a different path for trading off progress on the objective from the deterministic terms and the generation of noise. In SGD, increasing η speeds up the convergence encoded by the \mathbf{A} matrix but also increases the noise encoded by the \mathbf{B} matrix, and an optimal choice of η trades these off efficiently. In LA we have the additional option to tune the outer learning rate ν with similar consequences; increasing it improves deterministic progress but also increases noise. This gives us a two-dimensional space of tradeoffs between deterministic progress and noise generation. Increase in noise from a larger inner learning rate η can be offset by a smaller outer learning rate ν and vice versa.

For small learning rates these effects are redundant; if $\|\mathbf{B}\|_{\text{op}} \ll \|\mathbf{A}\|_{\text{op}}$ and $\eta \lambda S \ll 1$, then configurations with a fixed product $\nu \eta$ will give near-identical dynamics. For larger learning rates, such as those associated with optimal training, this is not the case. For example $\nu > 1$ decreases stability non-linearly (Appendix A.2). However, as we will show in the next section, nontrivial ν can bring net benefits to optimization.

3.2. Lookahead can optimize faster than SGD

An immediate question is: are there scenarios where nontrivial LA ($\nu \neq 1$) optimizes faster than SGD? More concretely, we consider the following scenario. Consider an initialization such that $\mathbf{p}_0 = \mathbf{A}^+ \mathbf{1}$ (corresponding to i.i.d. initialization of \mathbf{z}_0). Consider the loss $\mathcal{L}(\nu, \eta, S)$ after S steps of LA from this initialization (that is, $\mathcal{L}(\nu, \eta, S) = \frac{1}{D} \mathbf{1}^\top \mathbf{A}^\top \mathbf{p}_S$). Then we can ask the question: are there spectra \mathbf{A} such that $\mathcal{L}(\nu, \eta, S) < \mathcal{L}(1, \eta_{\text{SGD}}, S)$ for some ν and η for any η_{SGD} ? More formally, we seek a choice of NTK spectrum where there exists some $\nu \neq 1$ and η such that

$$\mathcal{L}(\nu, \eta, S) < \arg \min_{\eta'} \mathcal{L}(1, \eta', S). \quad (18)$$

Perhaps surprisingly, the answer is yes. We numerically iterated Equation 17 for a variety of spectra \mathbf{A} , batch fraction B/D , and sync cycle period S . For each such setting, we ran S steps of dynamics over a grid of η and ν values to calculate the change in loss after one cycle. As expected, we generally found that the optimal value of η for a particular ν decreased in ν (Figure 1, left).

We found that there were multiple settings for which the optimal (ν, η) pair involved $\nu > 1$. In general, variance in the spectrum causes the optimal ν to shift away from 1. For example, consider a ‘‘spiked spectrum’’ with two eigenval-

ues λ_0 (99% of eigenmodes) and $20\lambda_0$ (1% of eigenmodes). Plotting the loss after one cycle as a function of ν (optimizing η for each ν), we see that the optimal ν is greater than 1 (Figure 1, middle). We found other settings where the optimal $\nu < 1$, such as certain power law spectra (Figure 1, right, $\alpha = -1.5$).

We note that the total benefit of LA amounts to a 10 – 20% decrease in the loss per cycle in the settings we present here. We conjecture that LA can provide modest but bounded gains in more general settings. The largest benefits tend to occur for smaller batch fraction B/D and longer cycles S .

3.3. Dynamics of LA-DiLoCo

We can extend the analysis of LA to LA-DiLoCo— that is, LA-DiLoCo with SGD as both the inner and outer optimizer. Given R workers indexed by k , the dynamics is given by:

$$\psi_{t;k} := \theta_t \text{ (when } t//S = 0) \quad (19)$$

$$\psi_{t+1;k} - \psi_{t;k} = -\frac{\eta}{B} \mathbf{J}^\top \mathbf{P}_{t;k} \mathbf{z}(\psi_{t;k}) \text{ for } S \text{ steps} \quad (20)$$

$$\theta_{t+T} - \theta_t = \nu \left(\frac{1}{R} \sum_{k=1}^R \psi_{t+S;k} - \theta_t \right) \quad (21)$$

where the $\mathbf{P}_{t;k}$ are all i.i.d. distributed as the \mathbf{P} before. This is similar to the dynamics of LA, except there are R independent copies of the parameters that are propagated for S steps. The average of these parameters is then propagated to the outer optimizer. Here B is the batch size per-worker, so the total batch size across workers is RB .

In the linear regression setting, the dynamics can once again be written over function space and we can derive the high dimensional dynamics of \mathbf{p} (Appendix A.1):

$$\mathbf{p}_{t+S} = \left([(1-\nu)\mathbf{I} + \nu(\mathbf{I} - \eta\mathbf{\Lambda})^S]^2 + \frac{\nu^2}{R} [\mathbf{T}_S - (\mathbf{I} - \eta\mathbf{\Lambda})^{2S}] \right) \mathbf{p}_t \quad (22)$$

This is identical to the dynamics of LA, but with the noise reduced by R . This suggests that adding more workers with the same B is always beneficial to training in this setting.

A more interesting and practically relevant scenario is one where the *total batch size* remains fixed, while the number of workers is varied. This allows, for example, a comparison between data-parallel training and LA-DiLoCo style training. If $R > 1$ is optimal here it would suggest that even when synchronous training is no more costly than asynchronous training, it is beneficial to decouple the parameters across workers.

To analyze this setting, it is useful to examine the structure of the noise term — the only place where LA-DiLoCo departs from LA. It is informative to write the full noise term as a

power series. We note that \mathbf{T}_S can be written as the sum of all possible S -words made of products of \mathbf{A} and \mathbf{B} . We define the power series \mathbf{M}_s by

$$\mathbf{M}_s \equiv \sum_{\mathbf{W} \in \pi_s^S} \mathbf{W} \quad (23)$$

where π_s^S is the set of products of length S of \mathbf{A} and \mathbf{B} with exactly s copies of \mathbf{A} . We note that $\mathbf{M}_0 = (\mathbf{I} - \eta\mathbf{\Lambda})^{2S}$. A simple but tedious calculation shows us that for $s > 0$, \mathbf{M}_s can be written as $\frac{\eta^{2s}}{B^s} \tilde{\mathbf{M}}_s(\eta)$, where $\tilde{\mathbf{M}}_s$ is independent of B and R . This means that we can write:

$$\frac{\nu^2}{R} [\mathbf{T}_S - (\mathbf{I} - \eta\mathbf{\Lambda})^{2S}] = \sum_{s=1}^S a_s \tilde{\mathbf{M}}_s(\eta), \quad a_s \equiv \frac{\nu^2 \eta^{2s}}{RB^s} \quad (24)$$

In terms of the total batch size $B_{tot} = BR$, the coefficients are given by

$$a_s = \frac{R^{s-1}}{B_{tot}^s} \nu^2 \eta^{2s} \quad (25)$$

This shows that at the same *total batch size*, using multiple workers $R > 1$ (LA-DiLoCo) generates *more noise* than single worker LA at matching η and ν . This suggests that in this setting, using LA-DiLoCo does not improve optimization — unlike the benefit gained from switching to LA from SGD. This can be formally proven for isotropic data:

Theorem 3.1. *Consider the dynamics of Equation 22 for fixed ν and η . Suppose $\mathbf{\Lambda}$ has identical eigenvalues. Then, for fixed total batch size $B_{tot} \equiv BR$, the eigenvalues of the linear system strictly increase with R .*

See Appendix A.3 for the proof. We conjecture that similar results exist for other data distributions, but leave this to future work.

Equation 22 and the power series decomposition can also be used to derive the relationships between hyperparameters in the two methods. We first consider the simple case where $\eta\lambda S \ll 1$ and $\nu\eta\lambda S \ll 1$ for all eigenvalues λ in $\mathbf{\Lambda}$. In this setting the noise is small, and the dynamics is dominated by the deterministic term. The gradient varies slowly, and the update equation is approximately $\mathbf{p}_{t+S} \approx (1 - \nu\eta\mathbf{\Lambda})\mathbf{p}_t$. In this setting, keeping the product $\nu\eta$ constant preserves the dynamics, across values of η and R .

The more interesting case is where there is non-trivial noise. Consider two training scenarios: one with LA with learning rate pair (ν_{loc}, η_{loc}) and the other with LA-DiLoCo with R workers and learning rate pair (ν_{dil}, η_{dil}) . If the total batch size B_{tot} is fixed across the methods, we can compute the ratio of the power series coefficients a_s . The B_{tot} dependence vanishes and we are left with:

$$\frac{a_{s,dil}}{a_{s,loc}} = \left(\frac{\nu_{dil}}{\nu_{loc}} \right)^2 R^{s-1} \left(\frac{\eta_{dil}}{\eta_{loc}} \right)^{2s} \quad (26)$$

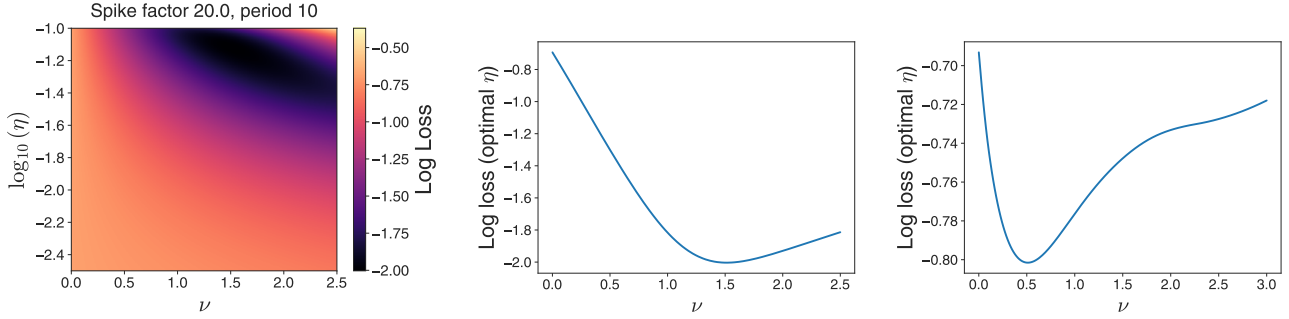


Figure 1. Loss after one cycle of $S = 10$ steps as a function of η and ν for spiked spectrum (left). Model has batch fraction $B/D = 0.2$, and spectrum has two eigenvalues λ_0 (99% of eigenmodes) and $20\lambda_0$ (1% of eigenmodes). Optimal $\eta^*(\nu)$ decreases in ν . Optimizing η for each ν reveals that the optimal ν is greater than 1 (middle). Power law spectrum with exponent $\alpha = -1.5$ has optimal $\nu < 1$ (right, $B/D = 0.005$).

This ratio can be set to 1 with the choice

$$\eta_{\text{dil}} = R^{-1/2} \eta_{\text{loc}}, \quad \nu_{\text{dil}} \eta_{\text{dil}} = \nu_{\text{loc}} \eta_{\text{loc}} \quad (27)$$

This suggests that one way to combat the increase in noise due to additional workers is to decrease the inner learning rate, but compensate by increasing the outer learning rate.

Note that even if $a_{s,\text{dil}} = a_{s,\text{loc}}$, the noise terms are not quite identical; in particular $\tilde{\mathbf{M}}_s$ depends on the learning rate via its $\mathbf{I} - \eta\mathbf{\Lambda}$ factors. As long as $\eta\lambda < 1$ for all λ in $\mathbf{\Lambda}$, the eigenvalues of $\tilde{\mathbf{M}}_s$ are increasing as η decreases. This means that LA-DiLoCo will still have more noise than LA even with the parameter matching. Also note that the deterministic term is also affected by changes in ν and $\mathbf{\Lambda}$ unless all eigenvalues are small. Therefore this learning rate scheme brings the dynamics of the two methods closer, but breaks down for large R and large η .

Nevertheless, this simple heuristic improves training outcomes in the linear regression setting. We trained models using LA-DiLoCo with various R across increasing inner learning rate η . We compared the scaling suggestion in Equation 27 to the baseline of not scaling η at all with R . The resulting curves show that using the same (ν, η) pairs across R causes discrepancies between the trajectories and larger R values diverge at relatively low values of η (Figure 2, top). In contrast, the heuristic $R^{-1/2}$ scaling (with counterscaling of ν) keeps learning trajectories approximately collapsed at small learning rates and keeps convergence at larger learning rates (Figure 2, bottom). Both figures show that the theory captures well the average loss trajectories of exact simulations.

In summary, our analysis suggests that at similar total batch sizes, synchronous training is favored over asynchronous training. However, the outer learning rate in LA-DiLoCo can partially compensate for the increased noise generation by using the theoretically motivated scaling rule.

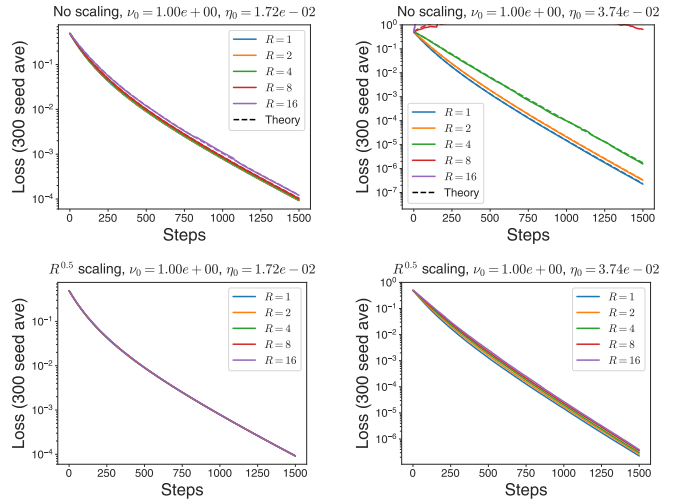


Figure 2. Averaged loss curves for LA diloco (solid lines) are well captured by theoretical model (dashed lines) across many settings with fixed total batch size (all panels, $D = 3200$, $B_{\text{tot}} = 64$, various learning rates). Keeping η and ν independent of number of workers R leads to similar dynamics at smaller learning rates (top left) but causes learning curves for larger R to diverge early at larger learning rates (top right). $R^{-1/2}$ scaling rule for η , with $\nu\eta$ fixed gives better correspondence across R for all learning rates (bottom), but dynamics still becomes non-universal at larger η (bottom right)

4. The benefits of dual momentum

In practical scenarios, DiLoCo is used with more complex optimizers in both the inner and outer loop. In particular, using momentum in both optimizers is crucial to successful methods.

In order to improve understanding of what momentum does in these methods, we analyze “Super”-Lookahead (SLA) — LA with SGD momentum in both the inner and outer optimizers. We focus on the deterministic setting to obtain interpretable results, but there is no in-principle issue with

extending the analysis to the stochastic high dimensional setting of the previous section (see Collins-Woodfin et al. (2024) for examples for other optimizers).

We directly analyze the eigenstructure of the per-cycle update, and show that the outer optimizer acts on a normalized, effective problem, and that the outer momentum can accelerate two types of eigenmodes — small eigenmodes corresponding to flat directions, and large eigenmodes near the edge of stability. Our analysis also shows that the particular form of momentum in the outer optimizer is crucial to success of the methods, and that Nesterov-style momentum is generally more effective than heavy ball. Overall the use of the second momentum non-linearly transforms the relationship between Hessian eigenvalues and convergence rate.

We note that our results are compatible with prior work which used worst-case analysis to analyze the effective condition number of related optimizers (Charles & Konečný, 2021; Charles & Rush, 2022). In both settings the authors found that the outer momentum acts on an “effective geometry” and changes the condition number in a non-linear fashion, and also derived improved bounds for Nesterov momentum.

4.1. Review of single momentum

We will briefly review the behavior of heavy ball and Nesterov momentum in our linear regression setting, in order to establish notation and build intuition for later analyses. EMA style momentum can be written as:

$$\zeta_{t+1} = (1 - \beta_1)\mathbf{g}_t + \beta_1\zeta_t \quad (28)$$

$$\theta_{t+1} = \theta_t - \eta\zeta_{t+1} \quad (29)$$

where \mathbf{g} is the gradient at θ . Similar to SGD, we can write the update equations in function space. For full batch GD on the linear regression setup, we have:

$$\mathbf{z}_{t+1} = (\mathbf{I} - \eta(1 - \beta_1)\hat{\Theta})\mathbf{z}_t - \eta\beta_1\mathbf{k}_t \quad (30)$$

$$\mathbf{k}_{t+1} = (1 - \beta_1)\hat{\Theta}\mathbf{z}_t + \beta_1\mathbf{k}_t \quad (31)$$

where \mathbf{k} is the momentum vector in function/data space. Note that we have written the equations to provide a simple linear recurrence relationship in $\mathbf{z} - \mathbf{k}$ space.

We can once again work in the eigenbasis of $\hat{\Theta}$ by rotating \mathbf{z} and \mathbf{k} . For each eigenvalue λ , the projections z and k of their respective eigenmodes evolve as

$$\begin{pmatrix} z_{t+1} \\ k_{t+1} \end{pmatrix} = \begin{pmatrix} 1 - \eta(1 - \beta_1)\lambda & -\eta\beta_1 \\ (1 - \beta_1)\lambda & \beta_1 \end{pmatrix} \begin{pmatrix} z_t \\ k_t \end{pmatrix} \quad (32)$$

The convergence rate of the eigenmode is determined by the magnitude of the largest eigenvalue ω_{\max} of the transition

matrix, since applying the transition matrix t times results in a total max eigenvalue of ω_{\max}^t . For convenience we define the convergence rate $r \equiv -\log(|\omega_{\max}|)$.

The eigenvalues ω_{\pm} are given by

$$\omega_{\pm} = \frac{1}{2} \left[(1 - \eta(1 - \beta_1)\lambda + \beta_1) \pm \sqrt{(1 - \eta(1 - \beta_1)\lambda + \beta_1)^2 - 4\beta_1} \right] \quad (33)$$

For small learning rates $\eta\lambda \ll 1 - \beta_1$ the largest eigenvalue is $\omega_+ \approx 1 - \eta\lambda$, with associated convergence rate $r = -\log(1 - \eta\lambda) \approx \eta\lambda$ —the same as SGD. The dynamics diverges for eigenvalues where $\eta\lambda > 2\frac{1+\beta_1}{1-\beta_1}$, allowing a maximal learning rate that is $\frac{1+\beta_1}{1-\beta_1}$ larger than GD. The ability to use this larger learning rate without sacrificing convergence of larger eigenmodes allows for faster convergence of smaller eigenmodes.

One interesting phenomenon induced by momentum is the existence of complex eigenmodes. These correspond to oscillatory modes whose convergence rate given by the norm of their eigenvalues $|\omega_{\pm}| = \sqrt{\beta_1}$ — which is independent of η and λ . If $\beta_1 = 1 - \delta$, $\delta \ll 1$ the convergence rate of the modes is $r \approx \delta/2$ — a potentially slow convergence. These modes occur when $(1 - \eta(1 - \beta_1)\lambda + \beta_1)^2 - 4\beta_1 < 0$, which for $1 - \beta_1 \ll 1$ corresponds to

$$\frac{1 - \beta_1}{4} < \eta\lambda < \frac{2(1 + \beta_1)}{1 - \beta_1} \quad (34)$$

That is, for β_1 close to 1 there is a range of $\eta\lambda$ spanning a factor of $O((1 - \beta_1)^{-2})$ which converge slowly. This is one of the issues with using β_1 too close to 1; even in this simple problem there is a tradeoff between stability and convergence rate that can't be mitigated through choice of learning rate.

Similarly, for Nesterov-style momentum we have:

$$\zeta_t = (1 - \beta_1)\mathbf{g}_t + \beta_1\zeta_{t-1} \quad (35)$$

$$\theta_{t+1} = \theta_t - \eta[(1 - \beta_1)\mathbf{g}_t + \beta_1\zeta_t] \quad (36)$$

In the eigenspace this nets the linear system

$$\begin{pmatrix} z_{t+1} \\ k_{t+1} \end{pmatrix} = \begin{pmatrix} 1 - (1 - \beta_1^2)\eta\lambda & -\eta\beta_1^2 \\ (1 - \beta_1)\lambda & \beta_1 \end{pmatrix} \begin{pmatrix} z_t \\ k_t \end{pmatrix} \quad (37)$$

This form is in units which matches the dynamics of EMA momentum for small eigenvalues $\eta\lambda \ll 1$. The traditional form can be recovered with the substitution $\tilde{\eta} := (1 - \beta_1)\eta$.

For this update rule, ω_{\pm} are complex when

$$\frac{(1 - \beta_1)}{(1 + \beta_1)^2} < \eta\lambda < \frac{1}{1 - \beta_1} \quad (38)$$

once again giving a range of $O((1 - \beta_1)^{-2})$ for complex eigenvalues. However, for Nesterov-style momentum the eigenvalue magnitude and convergence rate depend on $\eta\lambda$:

$$\begin{aligned} |\omega_{\pm}| &= \sqrt{\beta_1(1 - (1 - \beta_1)\eta\lambda)}, \\ r &= -\frac{1}{2} \log(\beta_1(1 - (1 - \beta_1)\eta\lambda)) \end{aligned} \quad (39)$$

For $\eta\lambda \ll (1 - \beta_1)^{-1}$ with complex eigenvalues we still have the same convergence issue as before; however, for $\eta\lambda \sim (1 - \beta_1)^{-1}$ (near the end of the complex region) the convergence is much improved. We will see in the next section that this makes Nesterov momentum uniquely suited to use in the outer optimizer of SLA.

4.2. SLA and dual momenta

We define the general Super Lookahead (SLA) optimizer as:

$$\psi_t := \theta_t \text{ (when } t//S = 0) \quad (40)$$

$$\psi_{t+1} - \psi_t = \text{InnerOpt}(\mathbf{g}(\psi_t)) \text{ for } S \text{ steps} \quad (41)$$

$$\theta_{t+T} = \theta_t - \text{OuterOpt}(\theta_t - \zeta_{t+T}) \quad (42)$$

where *InnerOpt* and *OuterOpt* are gradient based optimizers. The outer optimizer uses the difference $\theta_t - \zeta_{t+T}$ in place of a gradient.

We consider the case where *InnerOpt* and *OuterOpt* are GD with EMA style momentum. We have inner and outer learning rates η and ν as before, and now have inner and outer momentum parameters β_{in} and β_{out} . In this setting the function space updates can be written as:

$$\tilde{\mathbf{z}}_t := \mathbf{z}_t \text{ (when } t//S = 0) \quad (43)$$

$$\left. \begin{aligned} \tilde{\mathbf{z}}_{t+1} &= (\mathbf{I} - \eta(1 - \beta_{\text{in}})\hat{\Theta})\tilde{\mathbf{z}}_t - \eta\beta_{\text{in}}\tilde{\mathbf{k}}_t \\ \tilde{\mathbf{k}}_{t+1} &= (1 - \beta_{\text{in}})\hat{\Theta}\tilde{\mathbf{z}}_t + \beta_{\text{in}}\tilde{\mathbf{k}}_t \end{aligned} \right\} \text{ for } S \text{ steps} \quad (44)$$

$$\mathbf{k}_{t+T} = -(1 - \beta_{\text{out}})[\tilde{\mathbf{z}}_{t+T-1} - \mathbf{z}_t] + \beta_{\text{out}}\mathbf{k}_t \quad (45)$$

$$\mathbf{z}_{t+S} = \mathbf{z}_t - \nu\mathbf{k}_{t+T} \quad (46)$$

We note that only $\tilde{\mathbf{z}}_t$ is synced between cycles; $\tilde{\mathbf{k}}$ is only modified via the inner optimizer.

In this setting, momentum rules can be generally written as

$$\begin{pmatrix} \tilde{\mathbf{z}}_{t+S} \\ \tilde{\mathbf{k}}_{t+S} \\ \mathbf{z}_{t+S} \\ \mathbf{k}_{t+S} \end{pmatrix} = \mathbf{T}_{\text{sync}} \mathbf{T}_{\text{out}} \mathbf{T}_{\text{in}} \begin{pmatrix} \tilde{\mathbf{z}}_t \\ \tilde{\mathbf{k}}_t \\ \mathbf{z}_t \\ \mathbf{k}_t \end{pmatrix} \quad (47)$$

where \mathbf{T}_{in} represents the S steps of the inner optimizer, \mathbf{T}_{out} represents the outer optimizer step, and \mathbf{T}_{sync} represents the syncing of inner and outer optimizers (in this case, the syncing of $\tilde{\mathbf{z}}_t$ to \mathbf{z}_t at the end of the cycle). By analyzing the eigenvalues of the product $\mathbf{T}_{\text{tot}} \equiv \mathbf{T}_{\text{sync}} \mathbf{T}_{\text{out}} \mathbf{T}_{\text{in}}$, we can understand the convergence rates of SLA as a function of the optimizer parameters. Detailed expressions for the matrices can be found in Appendix B.1.

4.3. Analysis of a 2-dimensional reduction

In order to build intuition for the convergence behavior, it is useful to define a variant of the optimizer where the eigenvalues of \mathbf{T}_{tot} are analytically tractable. Consider the additional rule $\tilde{\mathbf{k}}_t := 0$ at the end of the S step cycle. This modifies \mathbf{T}_{sync} only.

Working once again in the $\hat{\Theta}$ eigenbasis, the dynamics per-cycle for each eigendirection can be described in terms of the projections z and k alone, since no information from $\tilde{\mathbf{z}}$ or $\tilde{\mathbf{k}}$ is carried over cycle-to-cycle. If we define \mathbf{T}_{in} as the block-diagonal matrix

$$\mathbf{T}_{\text{in}} = \begin{pmatrix} \mathbf{F} & 0 \\ 0 & \mathbf{I} \end{pmatrix}, \quad \mathbf{F} = \begin{pmatrix} 1 - (1 - \beta_{\text{in}})\eta\lambda & -\eta\beta_{\text{in}} \\ (1 - \beta_{\text{in}})\lambda & \beta_{\text{in}} \end{pmatrix}^S \quad (48)$$

then the update rule reduces to

$$\begin{pmatrix} z_{t+S} \\ k_{t+S} \end{pmatrix} = \begin{pmatrix} 1 - \nu(1 - \beta_{\text{out}})[1 - F_{11}] & -\nu\beta_{\text{out}} \\ (1 - \beta_{\text{out}})[1 - F_{11}] & \beta_{\text{out}} \end{pmatrix} \begin{pmatrix} z_t \\ k_t \end{pmatrix} \quad (49)$$

We immediately see that SLA amounts to doing Momentum-GD on an effective spectrum $1 - F_{11}$. Note that this structure holds for any inner optimizer whose S step optimization can be written as a linear function of z_t and k_t .

If $1 - F_{11} \ll 1$, then the corresponding convergence rate per-cycle is $r \approx \nu(1 - F_{11})$ — which suggests that an outer learning rate $\nu > 1$ can improve convergence. There are two main scenarios that lead to this case. The first is if $\eta\lambda S \ll 1$. In this case, $F_{11} \approx 1 - S\eta\lambda$. If we define the *per step* convergence rate $r \equiv -\frac{1}{S} \log(|\omega_{\max}|)$ for the largest eigenvalue of \mathbf{T}_{tot} , we have $r \approx \nu\eta\lambda$.

The second scenario is slow convergence due to large eigenvalues. For example if $\beta_{\text{in}} = 0$ (no inner momentum) and $\eta\lambda = 2 - \delta$ for $\delta \ll 1$, then $F_{11} \approx 1 - S\delta$ and the per-cycle convergence rate becomes $r \approx \nu\delta$ — again giving potential for acceleration via the outer learning rate. A similar effect applies to the inner eigenmodes with imaginary eigenvalues if $S(1 - \beta_{\text{in}}) \ll 1$, since those will converge slowly as well.

This analysis suggests that the second momentum, paired with $\nu > 1$, can improve improve convergence not only of small eigenmodes like the inner momentum, but oscillating and slowly converging eigenmodes at the edge of stability/in the critical damping regime.

However, there is one large downside: eigenmodes that are damped by the outer momentum (with the corresponding imaginary eigenvalues) will be slowed down. For $\beta_{\text{out}} = 1 - \delta$, $\delta \ll 1$ their per-step convergence rate will be $r = \frac{1}{S}(1 - \delta/2)$ — that is the per-step convergence rate is *smaller* for longer cycles. This is because their *per-cycle* convergence rate depends on the eigenvalue β_{out} .

This convergence issue is an even bigger problem in the

outer optimizer than the inner optimizer; any eigenmode that makes significant optimization progress in S steps will have small F_{11} . The best-optimizing eigenmodes in the inner optimizer can become the slowest in the outer optimizer. These results suggest that β_{out} will likely need to be even further from 1 than β_{in} .

These convergence issues can be greatly mitigated by using Nesterov-style momentum. The 2-d dynamics becomes:

$$\begin{pmatrix} z_{t+S} \\ k_{t+S} \end{pmatrix} = \begin{pmatrix} 1 - \nu(1 - \beta_{\text{out}}^2)(1 - F_{11}) & -\nu\beta_{\text{out}}^2 \\ (1 - \beta_{\text{out}})(1 - F_{11}) & \beta_{\text{out}} \end{pmatrix} \begin{pmatrix} z_t \\ k_t \end{pmatrix} \quad (50)$$

Once again, the effective eigenvalues are given by $1 - F_{11}$. This means that in the damped/complex eigenvalue regime, the per-cycle eigenvalue magnitude is $\sqrt{\beta_{\text{out}}(1 - (1 - \beta_{\text{out}})\nu(1 - F_{11}))}$. Any eigenvalues where $\nu(1 - F_{11}) \ll (1 - \beta_{\text{out}})^{-1}$ will still experience slowdown. Since $1 - F_{11} \in [0, 1]$ and $(1 - \beta_{\text{out}})^{-1} > 1$, the only hope to combat this is to pick $\nu \geq (1 - \beta_{\text{out}})^{-1}$ (corresponding to $\nu \geq 1$ with traditionally parameterized Nesterov momentum).

Unlike the inner optimizer, where the learning rate can only be tuned to accelerate a small range of eigenmodes (those with $\eta\lambda \sim (1 - \beta_{\text{in}})^{-1}$), there is a special value of ν that can mitigate the damping for many eigenmodes. The choice $\nu = (1 - \beta_{\text{out}})^{-1}$ accelerates all eigenmodes with effective eigenvalues $1 - F_{11} \approx 1$, or alternatively $F_{11} \ll 1$. There is a large class of eigendirections with this property: namely eigenmodes which make significant progress on the loss in a single cycle. These modes are normally damped by the outer optimizer, but with Nesterov momentum and a well-tuned outer learning rate the damping is mitigated. For example, if $F_{11} = ae^{-\lambda S}$ as S is varied, and $\nu = (1 - \beta_{\text{out}})^{-1}$, the convergence rate per cycle is $r > S\lambda$, and per step is $r > \lambda$.

Overall, this analysis shows that applying two momenta at different scales has non-trivial effects that can't be replicated by a single momentum. With the correct choice of momentum rule the outer momentum can speed up convergence of eigendirections slowed down by the inner momentum, while preserving progress on well-converging modes. This effect can't be captured by simple interventions like adding weight averaging on top of momentum (Appendix B.2) or proposed algorithms like GPA (Defazio et al., 2025) which try to capture some of the effects of SLA (Appendix B.3).

4.4. Numerical results

We analyzed convergence rates for EMA and Nesterov momenta by performing eigendecomposition of \mathbf{T}_{tot} for both the reduced system analyzed above, as well as the original system described by Equations 43 to 46 where $\tilde{\mathbf{k}}$ is not reset to 0 every cycle. We fixed $\eta = 1$, $\lambda = 0.2$, $\beta_{\text{in}} = 0.9$, $\beta_{\text{out}} = 0.8$, and kept the inner optimizer fixed to EMA

momentum. This put the inner optimizer in the imaginary eigenvalue regime. These values were chosen to illustrate our general points, which hold across a wide range of parameter values.

We found that the convergence rates of the reduced system and the original system are similar for larger S (Figure 3). Resetting $\tilde{\mathbf{k}}$ to 0 tends to improve the convergence rate for small S . If we set ν to a generic stable value, we see that the convergence rate for Nesterov is larger than the convergence rate for EMA momentum, by a fixed factor for large S (Figure 3, top). However we see that the per-step convergence rate decreases as $1/S$ because the per-cycle convergence rate is fixed, as predicted by the theory.

However, if we set ν to the critical value $(1 - \beta_{\text{out}})^{-1}$, then we see that the per-step convergence rate of Nesterov momentum goes to a constant as predicted (Figure 3, bottom). This highlights the point that the critical outer learning rate is useful for preserving convergence rates for large S .

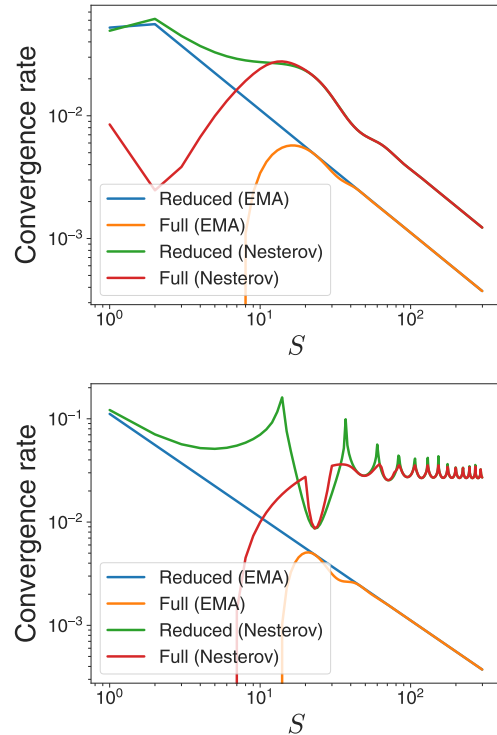


Figure 3. Eigenmodes damped by inner optimizer show decreasing per-step convergence rate with momentum-GD in the outer optimizer (top, $\nu = 2$). Convergence rate is improved for Nesterov momentum. At the critical $\nu = (1 - \beta_{\text{out}})^{-1}$, Nesterov convergence rate becomes S -invariant at large S (bottom). Reduced system with $\tilde{\mathbf{k}}_t := 0$ every cycle has similar behavior to full dynamics with $\tilde{\mathbf{k}}_t$ preserved for larger S , but shows faster convergence/better stability at smaller S . All experiments have $\eta = 1$, $\lambda = 0.2$, $\beta_{\text{in}} = 0.9$, $\beta_{\text{out}} = 0.8$.

5. Discussion

Our analysis of LA-DiLoCo and LA represents the first average case analysis of these algorithms in the high dimensional setting. These tools reveal the complex tradeoff between signal and noise that controls the convergence rates of the algorithms in this setting. Our results show that LA, even with a single worker, is quantitatively different from SGD and with sufficient eigenvalue dispersion can even optimize more quickly than SGD. Our analysis of LA-DiLoCo suggests that all else equal, synchronous optimizers are better than asynchronous ones, but it is possible to design good hyperparameter transfer schemes for a modest number of workers. Our analysis of the momentum-equipped SLA variants in the deterministic setting give new insights into the opportunities for acceleration, and suggest that Nesterov momentum minimizes the downsides of the approach — mirroring and perhaps explaining observations in practical settings (Charles et al., 2025; Kallusky et al., 2025).

Overall the benefits of two-phase optimizers in this setting come from the fact that the outer optimizer operates on an “effective” problem defined by the action of the inner optimizer. These benefits are due to new tradeoffs between speed and stability surfaced by the structure of the optimizer, that are easily accessible via hyperparameter tuning. These effects can’t be recreated with traditional optimizers equipped with weight averaging (Appendix B.2), nor by algorithms like GPA (Defazio et al., 2025) which seek to mimic the benefits of SLA (Appendix B.3).

The main weakness of our analysis is that it assumes the geometry of the loss landscape (e.g. the Hessian/NTK) is fixed. One next step would be to analyze cases where the eigenvalues and eigenvectors of the Hessian shift over time, or where the loss landscape is not well characterized by first and second derivatives on the scales relevant for the learning dynamics. In particular, it is known that algorithmic choices induce feedback on the large eigenvalues of the loss landscape (Cohen et al., 2021; 2022; Roulet et al., 2024); understanding how this phenomenon affects two-phase optimizers is likely crucial to improve these methods further, and scale them to larger workloads.

Our analysis suggests that the optimization dynamics of these two-phase optimizers has unique properties not found in most commonly used training algorithms. Though the periodic structure is an aesthetic departure from typical algorithms, the ability to explicitly access different time and curvature scales is robustly beneficial. We speculate that these effects can eventually be bridged with other methods that exploit multiple timescales (Defazio et al., 2024; Ferbach et al., 2025). The insights presented here are just the starting point to new exciting paradigms in training algorithms.

6. Acknowledgments

The author would like to thank Keith Rush and Zachary Charles for their help in learning about DiLoCo and other optimizers, and their guidance in preparing the manuscript.

References

- Agarwala, A. and Pennington, J. High dimensional analysis reveals conservative sharpening and a stochastic edge of stability. *arXiv preprint arXiv:2404.19261*, 2024.
- Charles, Z. and Konečný, J. Convergence and accuracy trade-offs in federated learning and meta-learning. In *International Conference on Artificial Intelligence and Statistics*, pp. 2575–2583. PMLR, 2021.
- Charles, Z. and Rush, K. Iterated vector fields and conservatism, with applications to federated learning. In Dasgupta, S. and Haghtalab, N. (eds.), *Proceedings of The 33rd International Conference on Algorithmic Learning Theory*, volume 167 of *Proceedings of Machine Learning Research*, pp. 130–147. PMLR, 29 Mar–01 Apr 2022. URL <https://proceedings.mlr.press/v167/charles22a.html>.
- Charles, Z., Teston, G., Dery, L., Rush, K., Fallen, N., Garrett, Z., Szlam, A., and Douillard, A. Communication-efficient language model training scales reliably and robustly: Scaling laws for diloco. *arXiv preprint arXiv:2503.09799*, 2025.
- Cohen, J. M., Kaur, S., Li, Y., Kolter, J. Z., and Talwalkar, A. Gradient descent on neural networks typically occurs at the edge of stability. *arXiv preprint arXiv:2103.00065*, 2021.
- Cohen, J. M., Ghorbani, B., Krishnan, S., Agarwal, N., Medapati, S., Badura, M., Suo, D., Cardoze, D., Nado, Z., Dahl, G. E., and Gilmer, J. Adaptive gradient methods at the edge of stability. *arXiv preprint arXiv:2207.14484*, 2022.
- Collins-Woodfin, E., Paquette, C., Paquette, E., and Seroussi, I. Hitting the high-dimensional notes: An ode for sgd learning dynamics on glms and multi-index models. *Information and Inference: A Journal of the IMA*, 13(4):iaae028, 2024.
- Defazio, A., Yang, X., Mehta, H., Mishchenko, K., Khaled, A., and Cutkosky, A. The road less scheduled. *Advances in Neural Information Processing Systems*, 37: 9974–10007, 2024.
- Defazio, A., Mishchenko, K., Raman, P., Shi, H.-J. M., and Xiao, L. Smoothing diloco with primal averaging for faster training of llms. *arXiv preprint arXiv:2512.17131*, 2025.

- Douillard, A., Feng, Q., Rusu, A. A., Chhaparia, R., Donchev, Y., Kuncoro, A., Ranzato, M., Szlam, A., and Shen, J. Diloco: Distributed low-communication training of language models. *arXiv preprint arXiv:2311.08105*, 2023.
- Douillard, A., Donchev, Y., Rush, J. K., Kale, S., Charles, Z., Teston, G., Garrett, Z., Shen, J., McIlroy, R., Lacey, D., Rame, A., Szlam, A., Ranzato, M., and Barham, P. R. Streaming diloco with overlapping communication. In *Second Conference on Language Modeling*, 2025. URL <https://openreview.net/forum?id=yYk3zK0X6Q>.
- Ferbach, D., Everett, K., Gidel, G., Paquette, E., and Paquette, C. Dimension-adapted momentum outpaces sgd. *arXiv preprint arXiv:2505.16098*, 2025.
- Jaghour, S., Ong, J. M., and Hagemann, J. Opendiloco: An open-source framework for globally distributed low-communication training, 2024. URL <https://arxiv.org/abs/2407.07852>.
- Kallusky, D., Rao, V., Nandavanam, V., and Shi, H.-J. M. Snoo: Step-k nesterov outer optimizer-the surprising effectiveness of nesterov momentum applied to pseudo-gradients. *arXiv preprint arXiv:2510.15830*, 2025.
- Khaled, A., Kale, S., Douillard, A., Jin, C., Fergus, R., and Zaheer, M. Understanding outer optimizers in local sgd: Learning rates, momentum, and acceleration. *arXiv preprint arXiv:2509.10439*, 2025.
- Lee, K., Cheng, A., Paquette, E., and Paquette, C. Trajectory of mini-batch momentum: batch size saturation and convergence in high dimensions. *Advances in Neural Information Processing Systems*, 35:36944–36957, 2022.
- Malinovskiy, G., Kovalev, D., Gasanov, E., Condat, L., and Richtarik, P. From local sgd to local fixed-point methods for federated learning. In *International Conference on Machine Learning*, pp. 6692–6701. PMLR, 2020.
- McMahan, B., Moore, E., Ramage, D., Hampson, S., and y Arcas, B. A. Communication-efficient learning of deep networks from decentralized data. In *Artificial intelligence and statistics*, pp. 1273–1282. PMLR, 2017.
- Reddi, S. J., Charles, Z., Zaheer, M., Garrett, Z., Rush, K., Konečný, J., Kumar, S., and McMahan, H. B. Adaptive federated optimization. In *International Conference on Learning Representations*, 2021. URL <https://openreview.net/forum?id=LkFG31B13U5>.
- Roulet, V., Agarwala, A., Grill, J.-B., Swirszcz, G., Blondel, M., and Pedregosa, F. Stepping on the edge: Curvature aware learning rate tuners. *Advances in Neural Information Processing Systems*, 37:47708–47740, 2024.
- Zhang, M., Lucas, J., Ba, J., and Hinton, G. E. Lookahead optimizer: k steps forward, 1 step back. *Advances in neural information processing systems*, 32, 2019.

A. High dimensional dynamics of LA and LA-DiLoCo

A.1. Derivation of the dynamics of \mathbf{p}

We derive the dynamics in the case of LA-DiLoCo here; LA is then the special case where $R = 1$. We have the dynamics:

$$\tilde{\mathbf{z}}_{t;k} := \mathbf{z}_t \text{ (when } t/S = 0) \quad (51)$$

$$\tilde{\mathbf{z}}_{t+1;k} - \tilde{\mathbf{z}}_{t;k} = -\eta \frac{D}{B} \hat{\Theta} \mathbf{P}_{t;k} \tilde{\mathbf{z}}_{t;k} \text{ for } S \text{ steps} \quad (52)$$

$$\mathbf{z}_{t+S} - \mathbf{z}_t = \frac{\nu}{R} \sum_{k=1}^R (\tilde{\mathbf{z}}_{t+S;k} - \mathbf{z}_t) \quad (53)$$

where the $\mathbf{P}_{t;k}$ are i.i.d. projection matrices with exactly B 1s on the diagonal and 0 everywhere else, for randomly chosen indices. The dynamics of the first moment of \mathbf{z} is given by:

$$\mathbb{E}[\mathbf{z}_{t+S} | \mathbf{z}_t] = \left[(1 - \nu) + \nu(1 - \eta \hat{\Theta}) \right] \mathbf{z}_t \quad (54)$$

The second moment evolves as

$$\mathbb{E}[\mathbf{z}_{t+S} \mathbf{z}_{t+S}^\top | \mathbf{z}_t] = \mathbb{E} \left[\left((1 - \nu) \mathbf{z}_t + \frac{\nu}{R} \sum_{k=1}^R \tilde{\mathbf{z}}_{t+S;k} \right) \left((1 - \nu) \mathbf{z}_t + \frac{\nu}{R} \sum_{k=1}^R \tilde{\mathbf{z}}_{t+S;k} \right)^\top \right] \quad (55)$$

Simplifying, we have:

$$\begin{aligned} \mathbb{E}[\mathbf{z}_{t+S} \mathbf{z}_{t+S}^\top | \mathbf{z}_t] &= (1 - \nu)^2 \mathbf{z}_t \mathbf{z}_t^\top + \frac{\nu(1 - \nu)}{R} \left(\sum_{k=1}^R \mathbb{E}[\tilde{\mathbf{z}}_{t+S;k} \mathbf{z}_t^\top + \mathbf{z}_t \mathbb{E}[\tilde{\mathbf{z}}_{t+S;k}^\top]] \right) \\ &\quad + \frac{\nu^2}{R^2} \sum_{j=1}^R \sum_{k=1}^R \mathbb{E}[\tilde{\mathbf{z}}_{t+S;j} \tilde{\mathbf{z}}_{t+S;k}^\top] \end{aligned} \quad (56)$$

Note that $\tilde{\mathbf{z}}_{t+S;j}$ and $\tilde{\mathbf{z}}_{t+S;k}$ are independent for $j \neq k$. We also note that the first and second moments of $\tilde{\mathbf{z}}_{t+S;k}$ given \mathbf{z}_t are identical to those of \mathbf{z}_{t+S} from SGD. We define:

$$\boldsymbol{\mu}_{t,s} \equiv \mathbb{E}_{\text{SGD}}[\mathbf{z}_{t+s} | \mathbf{z}_t], \quad \boldsymbol{\Sigma}_{t,s} \equiv \mathbb{E}_{\text{SGD}}[\mathbf{z}_{t+s} \mathbf{z}_{t+s}^\top | \mathbf{z}_t] \quad (57)$$

Then we have:

$$\mathbb{E}[\mathbf{z}_{t+S} \mathbf{z}_{t+S}^\top | \mathbf{z}_t] = (1 - \nu)^2 \mathbf{z}_t \mathbf{z}_t^\top + \nu(1 - \nu) (\boldsymbol{\mu}_{t,S} \mathbf{z}_t^\top + \mathbf{z}_t \boldsymbol{\mu}_{t,S}^\top) + \nu^2 \left(1 - \frac{1}{R} \right) \boldsymbol{\mu}_{t,S} \boldsymbol{\mu}_{t,S}^\top + \frac{1}{R} \boldsymbol{\Sigma}_{t,S} \quad (58)$$

Grouping terms by R we have:

$$\mathbb{E}[\mathbf{z}_{t+S} \mathbf{z}_{t+S}^\top | \mathbf{z}_t] = \left[(1 - \nu) \mathbf{z}_t + \nu \boldsymbol{\mu}_{t,S} \right] \left[(1 - \nu) \mathbf{z}_t + \nu \boldsymbol{\mu}_{t,S} \right]^\top + \frac{\nu^2}{R} (\boldsymbol{\Sigma}_{t,S} - \boldsymbol{\mu}_{t,S} \boldsymbol{\mu}_{t,S}^\top) \quad (59)$$

To obtain the dynamics of \mathbf{p}_t , we use the definition $\mathbf{p}_t \equiv \boldsymbol{\Lambda}^+ \text{diag}(\mathbf{V}^\top \mathbb{E}_{\mathbf{P}}[\mathbf{z}_t \mathbf{z}_t^\top] \mathbf{V})$ combined with the previous results from SGD. We have:

$$\boldsymbol{\mu}_{t,S} = (\mathbf{I} - \eta \hat{\Theta})^S \mathbf{z}_t, \quad \mathbf{V}^\top \boldsymbol{\mu}_{t,S} \boldsymbol{\mu}_{t,S}^\top \mathbf{V} = (\mathbf{I} - \eta \boldsymbol{\Lambda})^S \mathbf{V}^\top \mathbf{z}_t \mathbf{z}_t^\top \mathbf{V} (\mathbf{I} - \eta \boldsymbol{\Lambda})^S \quad (60)$$

which allows us to simplify the first two terms as

$$\boldsymbol{\Lambda}^+ \text{diag}(\mathbf{V}^\top \left[(1 - \nu) \mathbf{z}_t + \nu \boldsymbol{\mu}_{t,S} \right] \left[(1 - \nu) \mathbf{z}_t + \nu \boldsymbol{\mu}_{t,S} \right]^\top \mathbf{V}) = \left[(1 - \nu) \mathbf{I} + \nu (\mathbf{I} - \eta \boldsymbol{\Lambda})^S \right]^2 \mathbf{p}_t \quad (61)$$

In high dimensions, the results on SGD show that $\boldsymbol{\Sigma}_{t,S}$ transforms to $(\mathbf{A} + \mathbf{B})^S \mathbf{p}_t$, where

$$\mathbf{A} \equiv (\mathbf{I} - \eta \boldsymbol{\Lambda})^2, \quad \mathbf{B} \equiv \left(\frac{1}{B} - \frac{1}{D} \right) \eta^2 \boldsymbol{\Lambda} \mathbf{1} \mathbf{1}^\top \boldsymbol{\Lambda}. \quad (62)$$

This gives us the final equations for \mathbf{p}_t for LA-DiLoCo:

$$\mathbf{p}_{t+S} = \left([(1-\nu)\mathbf{I} + \nu(\mathbf{I} - \eta\mathbf{\Lambda})^S]^2 + \frac{\nu^2}{R} [\mathbf{T}_S - (\mathbf{I} - \eta\mathbf{\Lambda})^{2S}] \right) \mathbf{p}_t \quad (63)$$

where

$$\mathbf{T}_s \equiv (\mathbf{A} + \mathbf{B})^s = \left[(\mathbf{I} - \eta\mathbf{\Lambda})^2 + \left(\frac{1}{B} - \frac{1}{D} \right) \eta^2 \mathbf{\Lambda} \mathbf{1} \mathbf{1}^\top \mathbf{\Lambda} \right]^s \quad (64)$$

A.2. Deterministic dynamics

In the deterministic setting (full batch training), the update equation is:

$$\mathbf{p}_{t+1} = [(1-\nu)\mathbf{I} + \nu(\mathbf{I} - \eta\mathbf{\Lambda})^S]^2 \mathbf{p}_t \quad (65)$$

This diagonalizes in the eigenbasis. To understand convergence it is sufficient to analyze the 1-dimensional system:

$$p_{t+1} = [(1-\nu) + \nu(1-\eta\lambda)^S]^2 p_t \quad (66)$$

The dynamics is stable/convergent if and only if:

$$[(1-\nu) + \nu(1-\eta\lambda)^S]^2 < 1 \quad (67)$$

Let $a = ((1-\eta\lambda)^S) - 1$. Then we have:

$$(1 + a\nu)^2 < 1 \rightarrow -\frac{2}{\nu} < a < 0 \quad (68)$$

This gives us

$$1 - \frac{2}{\nu} < (1-\eta\lambda)^S < 1 \quad (69)$$

For $\nu = 1$, we recover the familiar $\eta\lambda < 2$ to prevent runaway growth. For even S , for $\nu < 2$ the condition is the same; after that the critical learning rate decreases with ν . For odd S , the condition is the same for all $\nu < 1$. For $\nu > 1$ gain the stable regime decreases. There is always some stable regime for all ν .

This analysis suggests that for $\nu < 1$, the stability of the inner SGD sets the stability of the overall dynamics. For larger ν , the training becomes harder to stabilize (requiring a smaller inner learning rate η), but there is always a convergent regime.

A.3. LA-DiLoCo slows convergence rates with isotropic data and fixed total batch size

Here we prove the following theorem:

Theorem 3.1. *Consider the dynamics of Equation 22 for fixed ν and η . Suppose $\mathbf{\Lambda}$ has identical eigenvalues. Then, for fixed total batch size $B_{\text{tot}} \equiv BR$, the eigenvalues of the linear system strictly increase with R .*

Proof. From Equation 22 that the dynamics of \mathbf{p} can be written as:

$$\mathbf{p}_{t+1} = \mathbf{F}(\eta, \nu, R, B_{\text{tot}}) \mathbf{p}_t \quad (70)$$

Our goal will be to show that \mathbf{F} has eigenvectors that are increasing in R when η , ν , and B_{tot} are fixed. Since \mathbf{F} is PSD, this also corresponds to slower convergence to 0 loss as R is varied. We can write:

$$\mathbf{F}(\eta, \nu, R, B_{\text{tot}}) = \mathbf{Q}(\eta, \nu) + \sum_{s=1}^S a_s(\eta, \nu, R, B_{\text{tot}}) \tilde{\mathbf{M}}_s(\eta) \quad (71)$$

where \mathbf{Q} and $\tilde{\mathbf{M}}$ are independent of R and B_{tot} . We will first show that each $\tilde{\mathbf{M}}_s(\eta)$ is PSD, and that a_s is increasing in R .

By definition, each $\tilde{\mathbf{M}}_s(\eta)$ can be written as a sum alternating products of matrices of the forms $\mathbf{\Lambda}$ and $\mathbf{\Lambda} \mathbf{1} \mathbf{1}^\top \mathbf{\Lambda}$. Since the data are isotropic, $\mathbf{\Lambda}$ is proportional to the identity and commutes with $\mathbf{\Lambda} \mathbf{1} \mathbf{1}^\top \mathbf{\Lambda}$. Therefore the $\tilde{\mathbf{M}}_s(\eta)$ are sums products of commuting PSD matrices, which are PSD, so $\tilde{\mathbf{M}}_s(\eta)$ are also PSD.

Recall that in this setting,

$$a_s(\eta, \nu, R, B_{\text{tot}}) = \frac{R^{s-1}}{B_{\text{tot}}^s} \nu^2 \eta^{2s} \quad (72)$$

Since the power series starts at $s = 1$, for all valid indices for any $0 < R_1 < R_2$, we have:

$$a_s(\eta, \nu, R_2, B_{\text{tot}}) \geq a_s(\eta, \nu, R_1, B_{\text{tot}}) \quad (73)$$

This means that we have:

$$\mathbf{F}(\eta, \nu, R_2, B_{\text{tot}}) - \mathbf{F}(\eta, \nu, R_1, B_{\text{tot}}) = \sum_{s=1}^S c_s \tilde{\mathbf{M}}_s(\eta) \quad (74)$$

for coefficients $c_s \geq 0$. Therefore, we can write:

$$\mathbf{F}(\eta, \nu, R_2, B_{\text{tot}}) = \mathbf{F}(\eta, \nu, R_1, B_{\text{tot}}) + \mathbf{U} \quad (75)$$

for a PSD matrix \mathbf{U} . By the properties of PSD matrices, $\lambda_{k,R_2} > \lambda_{k,R_1}$ where $\lambda_{k,R}$ is the k th eigenvalue of $\mathbf{F}(\eta, \nu, R, B_{\text{tot}})$, thus proving the theorem. \square

This proof technique does not immediately work for non-isotropic $\mathbf{\Lambda}$ since in that case, the individual summands of the $\tilde{\mathbf{M}}_s(\eta)$ are not PSD. However our numerical results lead us to conjecture that a weaker version of the theorem holds for more general distributions, perhaps restricted to the maximum eigenvalue of the $\mathbf{F}(\eta, \nu, R, B_{\text{tot}})$. We leave explorations of this direction to future work.

B. Deterministic dynamics of SLA

In this section we derive the deterministic dynamics of SLA in the linear setting, and show how the dynamics are different from weight averaging and GPA.

B.1. Full linear dynamics

In the deterministic setting of the linear regression problem (full batch size), we can write the SLA dynamics in function space as:

$$\begin{pmatrix} \tilde{\mathbf{z}}_{t+S} \\ \tilde{\mathbf{k}}_{t+S} \\ \mathbf{z}_{t+S} \\ \mathbf{k}_{t+S} \end{pmatrix} = \mathbf{T}_{\text{sync}} \mathbf{T}_{\text{out}} \mathbf{T}_{\text{in}} \begin{pmatrix} \tilde{\mathbf{z}}_t \\ \tilde{\mathbf{k}}_t \\ \mathbf{z}_t \\ \mathbf{k}_t \end{pmatrix} \quad (76)$$

Here \mathbf{T}_{in} and \mathbf{T}_{out} represent the inner and outer optimizers respectively, and \mathbf{T}_{sync} represents the ‘‘syncing’’ operation that prepares \mathbf{z} and \mathbf{k} for the next cycle.

The standard definition of SLA which only syncs \mathbf{z} has the syncing operator:

$$\mathbf{T}_{\text{sync}} = \begin{pmatrix} 0 & 0 & \mathbf{I} & 0 \\ 0 & \mathbf{I} & 0 & 0 \\ 0 & 0 & \mathbf{I} & 0 \\ 0 & 0 & 0 & \mathbf{I} \end{pmatrix} \quad (77)$$

while the 2-D simplification where \mathbf{k}_t is initialized to 0 every cycle has the operator:

$$\mathbf{T}_{\text{sync}} = \begin{pmatrix} 0 & 0 & \mathbf{I} & 0 \\ 0 & 0 & 0 & 0 \\ 0 & 0 & \mathbf{I} & 0 \\ 0 & 0 & 0 & \mathbf{I} \end{pmatrix} \quad (78)$$

For EMA style momentum, the inner and outer optimizer are given by the operators

$$\mathbf{T}_{\text{in}} = \begin{pmatrix} \mathbf{I} - \eta(1 - \beta_{\text{in}}) \frac{1}{D} \hat{\Theta} & -\eta \beta_{\text{in}} \mathbf{I} & 0 & 0 \\ (1 - \beta_{\text{in}}) \frac{1}{D} \hat{\Theta} & \beta_{\text{in}} \mathbf{I} & 0 & 0 \\ 0 & 0 & \mathbf{I} & 0 \\ 0 & 0 & 0 & \mathbf{I} \end{pmatrix}^S, \quad \mathbf{T}_{\text{out}} = \begin{pmatrix} \mathbf{I} & 0 & 0 & 0 \\ 0 & \mathbf{I} & 0 & 0 \\ \nu(1 - \beta_{\text{out}}) \mathbf{I} & 0 & \mathbf{I} - \nu(1 - \beta_{\text{out}}) \mathbf{I} & -\nu \beta_{\text{out}} \mathbf{I} \\ -(1 - \beta_{\text{out}}) \mathbf{I} & 0 & (1 - \beta_{\text{out}}) \mathbf{I} & \beta_{\text{out}} \mathbf{I} \end{pmatrix} \quad (79)$$

while for Nesterov (in EMA units) we have

$$\mathbf{T}_{\text{in}} = \begin{pmatrix} \mathbf{I} - \eta(1 - \beta_{\text{in}}^2)\frac{1}{D}\hat{\Theta} & -\eta\beta_{\text{in}}^2\mathbf{I} & 0 & 0 \\ (1 - \beta_{\text{in}})\frac{1}{D}\hat{\Theta} & \beta_{\text{in}}\mathbf{I} & 0 & 0 \\ 0 & 0 & \mathbf{I} & 0 \\ 0 & 0 & 0 & \mathbf{I} \end{pmatrix}^S, \quad \mathbf{T}_{\text{out}} = \begin{pmatrix} \mathbf{I} & 0 & 0 & 0 \\ 0 & \mathbf{I} & 0 & 0 \\ \nu(1 - \beta_{\text{out}}^2)\mathbf{I} & 0 & \mathbf{I} - \nu(1 - \beta_{\text{out}}^2)\mathbf{I} & -\nu\beta_{\text{out}}^2\mathbf{I} \\ -(1 - \beta_{\text{out}})\mathbf{I} & 0 & (1 - \beta_{\text{out}})\mathbf{I} & \beta_{\text{out}}\mathbf{I} \end{pmatrix} \quad (80)$$

We can once again shift to the eigenbasis of $\frac{1}{D}\hat{\Theta}$. This reduces the dynamics to a 4-dimensional system for each eigenmode. For EMA momentum, for example, we have:

$$\mathbf{T}_{\text{in}} = \begin{pmatrix} 1 - (1 - \beta_{\text{in}})\eta\lambda & -\eta\beta_{\text{in}} & 0 & 0 \\ (1 - \beta_{\text{in}})\lambda & \beta_{\text{in}} & 0 & 0 \\ 0 & 0 & 1 & 0 \\ 0 & 0 & 0 & 1 \end{pmatrix}^S, \quad \mathbf{T}_{\text{out}} = \begin{pmatrix} 1 & 0 & 0 & 0 \\ 0 & 1 & 0 & 0 \\ \nu(1 - \beta_{\text{out}}) & 0 & 1 - \nu(1 - \beta_{\text{out}}) & -\nu\beta_{\text{out}} \\ -(1 - \beta_{\text{out}}) & 0 & (1 - \beta_{\text{out}}) & \beta_{\text{out}} \end{pmatrix} \quad (81)$$

The inner and outer optimizers have a block diagonal structure:

$$\mathbf{T}_{\text{in}} = \begin{pmatrix} \mathbf{F} & 0 \\ 0 & \mathbf{I} \end{pmatrix}, \quad \mathbf{T}_{\text{out}} = \begin{pmatrix} \mathbf{I} & 0 \\ \mathbf{G} & \mathbf{H} \end{pmatrix}, \quad \mathbf{T}_{\text{out}}\mathbf{T}_{\text{in}} = \begin{pmatrix} \mathbf{F} & 0 \\ \mathbf{GF} & \mathbf{H} \end{pmatrix} \quad (82)$$

which for EMA momentum gives

$$\mathbf{F} = \begin{pmatrix} 1 - (1 - \beta_{\text{in}})\eta\lambda & -\eta\beta_{\text{in}} \\ (1 - \beta_{\text{in}})\lambda & \beta_{\text{in}} \end{pmatrix}^S, \quad \mathbf{G} = \begin{pmatrix} \nu(1 - \beta_{\text{out}}) & 0 \\ -(1 - \beta_{\text{out}}) & 0 \end{pmatrix}, \quad \mathbf{H} = \begin{pmatrix} 1 - \nu(1 - \beta_{\text{out}}) & -\nu\beta_{\text{out}} \\ (1 - \beta_{\text{out}}) & \beta_{\text{out}} \end{pmatrix} \quad (83)$$

The \mathbf{F} matrix is of particular interest, as it defines the ‘‘effective spectrum’’ seen by the outer optimizer in the linear regression setting.

B.2. Momentum with weight averaging

Our analysis of SLA in the deterministic linear regression setting begs the immediate question: are there algorithms which don’t have the two-phase structure, but have similar behavior after S steps? While this question is still generally open, we can answer in the negative for the most basic idea: pairing the dynamics of SGD momentum with an exponential moving average of the parameters.

Consider the deterministic setting of the linear regression problem. In the diagonalized basis, given an eval point \hat{z} which is an EMA of z with coefficient β_{ema} (where $\beta_{\text{ema}} = 0$ corresponds to normal evaluation at the latest parameter value), the update rule for the 3-dimensional system becomes:

$$\begin{pmatrix} z_{t+1} \\ k_{t+1} \\ \hat{z}_{t+1} \end{pmatrix} = \begin{pmatrix} 1 & 0 & 0 \\ 0 & 1 & 0 \\ 1 - \beta_{\text{ema}} & 0 & \beta_{\text{ema}} \end{pmatrix} \begin{pmatrix} 1 - \eta(1 - \beta_1)\lambda & -\eta\beta_1 & 0 \\ (1 - \beta_1)\lambda & \beta_1 & 0 \\ 0 & 0 & 1 \end{pmatrix} \begin{pmatrix} z_t \\ k_t \\ \hat{z}_t \end{pmatrix} \quad (84)$$

Evaluating we have:

$$\begin{pmatrix} z_{t+1} \\ k_{t+1} \\ \hat{z}_{t+1} \end{pmatrix} = \begin{pmatrix} 1 - \eta(1 - \beta_1)\lambda & -\eta\beta_1 & 0 \\ (1 - \beta_1)\lambda & \beta_1 & 0 \\ (1 - \beta_{\text{ema}})[1 - \eta(1 - \beta_1)] & -(1 - \beta_{\text{ema}})\eta\beta_1 & \beta_{\text{ema}} \end{pmatrix} \begin{pmatrix} z_t \\ k_t \\ \hat{z}_t \end{pmatrix} \quad (85)$$

Since \hat{z} depends on z and k , but does not causally affect them, two of the eigenvalues of this system are the eigenvalues of the original system. This can be seen directly by the fact that there are two left eigenvectors of the transition matrix which lie in the z/k subspace alone. These eigenvectors have the same eigenvalues as the original problem. The remaining eigenvalue has eigenvalue β_{ema} , since the trace of the new system is the trace of the old system plus β_{ema} .

This means that EMA of the evaluation point does not appreciably change the eigenstructure of the problem in the same way that SLA does via the outer momentum applied to the ‘‘effective’’ problem.

B.3. GPA in linear regression

The GPA algorithm in Defazio et al. (2025) (and indeed, the paper title) is partially inspired by coming up with an alternative of single-worker DiLoCo which maintains its benefits, but doesn't require the very discrete structure of the two-phase optimization process. The paper suggests that GPA can be thought of as a continuous relaxation of DiLoCo. Here we show that in the deterministic setting, SLA and GPA have quite different dynamics.

The original GPA formulation can be defined by the following equations:

$$y_t = \mu_y x_t + (1 - \mu_y) z_t \quad (86)$$

$$z_{t+1} = z_t + \eta_t d(y_t) \quad (87)$$

$$x_{t+1} = \mu_x x_t + (1 - \mu_x) z_{t+1} \quad (88)$$

Here $d(y_t)$ represents the ‘‘update’’ of a base optimizer - for example, the negative gradient in the case of SGD. The variable x_t is used for evaluation.

To understand the dynamics, we first re-write everything so that we have equations for y_{t+1} , z_{t+1} , and x_{t+1} as functions of y_t , z_t , and x_t only. This gives us:

$$y_{t+1} = \mu_x x_{t+1} + (1 - \mu_y) z_{t+1} = \mu_y \mu_x x_t + \mu_y (1 - \mu_x) z_{t+1} + (1 - \mu_y) z_{t+1} \quad (89)$$

$$y_{t+1} = \mu_x \mu_y x_t + (1 - \mu_x \mu_y) [z_t + \eta_t d(y_t)] \quad (90)$$

The corresponding x and z equations are simple to compute, and we end up with:

$$\begin{pmatrix} y_{t+1} \\ z_{t+1} \\ x_{t+1} \end{pmatrix} = \begin{pmatrix} 0 & 1 - \mu_x \mu_y & \mu_x \mu_y \\ 0 & 1 & 0 \\ 0 & 1 - \mu_x & \mu_x \end{pmatrix} \begin{pmatrix} y_t \\ z_t \\ x_t \end{pmatrix} + \eta_t d(y_t) \begin{pmatrix} 1 - \mu_x \mu_y \\ 1 \\ 1 - \mu_x \end{pmatrix} \quad (91)$$

In the deterministic setting of the linear regression model, the optimization problem decomposes over the eigenmodes and we have $d(y_t) = -\lambda y_t$. This gives us:

$$\begin{pmatrix} y_{t+1} \\ z_{t+1} \\ x_{t+1} \end{pmatrix} = \begin{pmatrix} -\eta_t \lambda (1 - \mu_x \mu_y) & 1 - \mu_x \mu_y & \mu_x \mu_y \\ -\eta_t \lambda & 1 & 0 \\ -(1 - \mu_x) \eta_t \lambda & 1 - \mu_x & \mu_x \end{pmatrix} \begin{pmatrix} y_t \\ z_t \\ x_t \end{pmatrix} \quad (92)$$

This has very different properties from any of the SLA matrices we analyzed in Section 4, particularly in how λ , η , and the other hyperparameters fold in to the overall spectrum. There is no clear ‘‘effective problem’’ dominating the eigenstructure like in SLA.

Another way we can see this is by changing variables. We define:

$$\hat{k}_t \equiv \frac{1}{\mu_x \mu_y} (-y_t + (1 - \mu_x \mu_y) z_t + \mu_x \mu_y x_t) \quad (93)$$

Then the dynamics of y_t and \hat{k}_t close and we have:

$$\hat{k}_{t+1} = \mu_x \hat{k}_t + (1 - \mu_x) \eta_t d(y_t) \quad (94)$$

$$y_{t+1} = y_t + \mu_y \hat{k}_{t+1} + (1 - \mu_y) \eta_t d(y_t) \quad (95)$$

We can see that this is very similar to Nesterov momentum, with an additional hyperparameter that decouples the contribution of the momentum and gradient to the parameter update. This also will have very different eigenstructure from SLA with Nesterov outer; in particular, it misses the interaction between the outer momentum and highly convergent eigenmodes seen in SLA. This suggests that the two algorithms are indeed qualitatively different.